18th International Conference on Structural Mechanics in Reactor Technology (SMiRT 18)
Beijing, China, August 7-12, 2005
SMiRT18-J07-1

FLUID-ELASTIC INSTABILITY OF TUBE BUNDLES IN TWO-PHASE CROSS-FLOW

I.-C. Chu, H. J. Chung

Korea Atomic Energy Research Institute
150 Dukjin-dong Yusong-gu Daejon Korea, 305-353
Phone: +82-42-868-2845, Fax: +82-42-861-6438
E-mail: chuic@kaeri.re.kr

ABSTRACT

Fluid-elastic instability characteristics in air-water two-phase cross-flow have been experimentally investigated using three different arrays of straight tube bundles. Rotated triangular array tube bundle with p/d of 1.47 is for the counterpart test of existing work. Rotated square and normal square array tube bundles with p/d of 1.633 are for the investigation of fluid-elastic instability features in KSNP steam generator. The present paper provides the experimental results of tube vibration response, damping ratio, hydrodynamic mass, and fluid-elastic instability. The damping ratio was very dependent on void fraction, as were in previous works. The tube vibration motion in the present rotated square array was quite different showing very weak tube-to-tube hydrodynamic coupling, which might result in very high fluid-elastic instability constant.

Keywords: Fluid-Elastic Instability, Damping Ratio, Hydrodynamic Mass, Two-Phase Cross-Flow.

1. INTRODUCTION

The U-bend region of nuclear steam generator tubes which undergoes high flow two-phase flow condition is highly susceptible to flow-induced vibration. In various flow-induced vibration mechanisms, it is generally known that fluid-elastic instability is the main cause of fretting wear of U-tubes.

In many comprehensive studies of fluid-elastic instability of the tube bundles in two-phase cross flow so far, considerable progress has been made by Pettigrew et al. (1989a, 1989b, 1995, 2001). One of the most important finding is that above a certain void fraction the critical flow velocity for the fluid-elastic instability becomes much lower than expected by the typical Connors' relation. They explained that this phenomenon is probably due to the flow regime transition from continuous bubbly flow to intermittent flow.

Their finding has a significant effect on the design of heat exchangers and nuclear steam generators however it has not been validated or confirmed by other's experiments yet. Moreover, most of the previous experiments were performed with tube bundles which had triangular or normal square arrays and p/d ratio under 1.5. According to Pettigrew et al. (2001), the fluid-elastic instability constant (K) has different value with regard to the tube array type and p/d ratio.

The U-bend region of KSNP (Korea Standard Nuclear Power Plant) steam generator has rotated square array with p/d of 1.633, which needs additional fluid-elastic instability experiments.

The main objectives of the present study are to cross-check the effect of the intermittent flow and to investigate the fluid-elastic instability characteristic in tube bundle equivalent to KSNP steam generator.

2. EXPERIMENTS

2.1 Test Facility

Figure 1 shows the schematic of the present test facility, which consists of test section, water supply system, air supply system, and measurement and control system.

The test section has cross-sectional dimension of 88×600 mm. As working fluids, air and water of atmospheric pressure and room temperature are injected at the bottom part of the test section. Cantilevered straight tube bundles are inserted into the rectangular flow channel at the downstream of about 1000 mm from the air and water injection point. A two-phase mixer and homogenizer are installed at the upstream of tube bundle to provide a uniform and homogeneous two-phase cross-flow.

Fluid-elastic instability characteristic have been experimentally investigated using three different tube bundles. That is, as shown in Fig. 2, rotated triangular array with p/d of 1.47, normal square array and rotated square array with p/d of 1.633. Each tube bundle is assembled with brass tube which has length of 600 mm, diameter of 12.7 mm, and thickness of 0.89 mm. The rotated triangular array has the same p/d ratio and the same dimensional tubes with Pettigrew et al. (1989a, 1989b).

Half-tubes are installed on both side walls of the flow channel to minimize the wall effect on the flow distribution (see Fig. 2). Visual observation of flow condition is possible through the both side walls and the tube end wall (the opposite of cantilevered side).

Three different array of dummy tube bundles are installed just upstream of each cantilevered tube bundle to provide more stable two-phase flow in each cantilevered tube bundle. Both ends of tubes in dummy bundles are tightly fixed.

Each cantilevered tube can vibrate in a cantilevered mode (flexible tube) or in a both side clamped mode (rigid tube). The tube bundle with all flexible tubes (flexible tube bundle) is used for the tests to find the onset of fluid-elastic instability, and the tube bundle with single flexible tube surrounded by rigid tube (rigid tube bundle) is used for the tests to measure the damping ratio and the hydrodynamic mass.

The tube vibration response of the single flexible tube was measured with a pair of orthogonally installed strain gages: each for the vibration measurement in drag and lift direction, respectively.

The water pump has the capacity of 100 m^3/hr at 50 m water head, and the air blower has the capacity of 6.5 m^3/min at discharge pressure of 2.6 bar. The water and air injection flow rate are mainly controlled by VVVF inverters.

2.2 Test Procedure

Experiments have been separately performed to find out the onset condition of fluid-elastic instability and to measure the damping and the hydrodynamic mass.

For the onset of fluid-elastic instability tests, homogeneous two-phase mass flux (or homogeneous gap velocity) was increased until the tube vibration amplitudes were significantly high to indicate the fluid-elastic instability while keeping the homogeneous void fraction constant for each flow rate. The flow rate was increased in sufficiently small steps to distinguish clearly the onset of instability.

Damping and hydrodynamic mass tests were performed at the same time under approximately half of the mass flux of the fluid-elastic instability conditions for given void fractions.

3. EXPERIMENTAL RESULTS

3.1 Flow Patterns

Flow patterns were visually observed and video recorded through the transparent window at the free vibrating tube end and the side window. The observed flow patterns were continuous bubbly flow, bubbly flow with some oscillations, and intermittent flow.

The continuous bubbly flow was observed below the homogeneous void fraction of about 80%, and the flow transition to the intermittent flow occurred when the void fraction was approximately above 90%. In addition, the void fraction of 90% for flow transition was almost regardless of tube bundle array.

The bubbly flow with some flow oscillation occurred below the void fraction of about 80% and at a certain higher homogeneous mass flux condition. For this flow regime, the continuous bubbly flow is instantaneously collapsed in some region resulting in the increased liquid portion which is then swept out by the following two-phase bubbly flow within very short duration. However the oscillation characteristics are quite different from that of intermittent flow, and the dominant flow regime could be identified as bubbly flow.

3.2 Vibration Response Characteristics

Figures 3~5 show the RMS tube displacement in the rotated triangular (RT) array, the normal square (NS) array, and the rotated square (RS) array under two-phase cross-flow, respectively. Tests were performed using flexible tube bundles.

When the homogeneous gap velocity is low, tube vibration responds show the turbulence-induced excitation characteristics. The tube vibration amplitude is similar both in drag and lift directions or slightly larger in drag direction, and the increase rate of RMS tube displacement with regard to the gap velocity is not significant.

Above a certain gap velocity, the RMS tube displacement shows a sharp increase with respect to small increase in the gap velocity, which can be defined as the critical gap velocity of fluid-elastic instability. In the case of RT and NS arrays, the sharp increases of tube displacement are found in lift direction.

On the contrary, fluid-elastic instability is found in drag direction in RS array, and the tube displacement in lift direction is low even for the very high gap velocities. Above the void fraction of 80% (80%, 90%, 95%), fluid-elastic instability was not found both in drag and lift directions even for the maximum achievable gap velocities of 4.2~4.3 m/s which was much higher than the critical gap velocities in the existing similar experiments.

Throughout the visual observation and video recording analysis of tube vibration motion, it can be definitively found that strong hydrodynamic coupling exists between neighboring tubes near the critical gap velocity in RT and NS arrays. On the other hand, the hydrodynamic coupling is very weak in RS array even above the critical gap velocity.

Figures 6 and 7 show the time-domain tube vibration waveform in RS and NS arrays for void fraction of 70% and gap velocity near the critical velocity. The tube vibration in NS array shows harmonic oscillation motion. On the other side, the tube vibration in RS array shows irregular up and down motion as if there was only the single tube in free stream flow.

However, the tube vibration of RS array in single phase water flow showed strong hydrodynamic coupling between neighboring tubes around the critical gap velocity. In addition, the vortex shedding peak and the fluid-elastic instability were observed in lift direction.

The most unique feature of the tube vibration motion in RS array with p/d of 1.633 is that the tube-to-tube interaction due to the hydrodynamic coupling between neighboring tubes is much weaker in two-phase flow condition, comparing to the single phase water flow in the same RS array and the two-phase flow in RT array with p/d of 1.47 and NS array with p/d of 1.633.

3.3 Damping Ratio

Basically, measurements of damping ratio in two-phase cross-flow were carried out about half the mass flux for the fluid-elastic instability conditions using rigid tube bundles, which follows the measurement procedure of Pettigrew et al. (1989a). Power spectral density (PSD) function was obtained from 30 min record of time domain vibration waveforms. Total damping ratio was evaluated using half power frequency band method.

Figures 8 and 9 show the PSD function in drag direction obtained for NS and RS arrays. In the case of NS array, only the vibration component at the natural frequency can be seen in drag and lift directions. However, significant low frequency vibration component exists in drag direction of RS array which is due to the irregular up and down motion.

In the case of RS array for void fraction of 60~70 %, the PSD peaks in drag direction and in lift direction became significantly broadened and slightly narrowed respectively as the mass flux increased in the range of 1/4~1/2 of the critical mass flux. As a result, the average total damping ratio increased significantly with respect to the mass flux. However, above the void fraction of 80%, the total damping ratio showed little change in drag and lift directions with regard to the mass flux increase.

Figure 10 shows the total damping ratio obtained for RT, NS, RS tube bundle arrays. The damping ratio was strongly dependent on the void fraction as noted by Pettigrew et al. (1989a), and it has the maximum at the void fraction of 60~70%.

3.4 Hydrodynamic Mass

Hydrodynamic mass has been evaluated from the following equation suggested by Carlucci and Brown (1983):

$$m_h = m_t\left(\left(f_g / f\right)^2 - 1\right) \tag{1}$$

where m_t is the mass per unit length of the tube alone, and f_g and f are the tube frequencies in air and in two-phase flow, respectively. The tube frequencies are obtained from the power spectral density functions which are used for damping calculation. Hydrodynamic mass can be measured at the same time for damping ratio measurement.

Figure 11 shows the measured hydrodynamic mass ratio in RT, NS, RS tube bundle arrays, and compares the present results with Pettigrew et al.'s data (1989a) and theoretical values. The present hydrodynamic mass data in RT array agree well with the data of Pettigrew et al. (1989a).

Hydrodynamic mass ratio in Fig. 11 is defined as the measured hydrodynamic mass in two-phase flow over the calculated hydrodynamic mass in water flow from Eq. (2).

The hydrodynamic masses in RS array are much lower than those in RT and NS arrays, which means lower liquid hold-up around tubes. This may have some relationship with the weak tube-to-tube hydrodynamic coupling in RS array with p/d of 1.633.

The hydrodynamic mass in RS array has been measured at about half and quarter of the critical mass flux or the maximum achievable mass flux, as in the case of damping measurement. Hydrodynamic masses measured at half of the critical mass flux are about 20% lower than those measured at quarter of the critical mass flux. The data in Fig. 11 correspond to the values measured at half of the critical mass flux.

Theoretical hydrodynamic mass is evaluated from the following equations presented in the work of Pettigrew et al.'s (1989a), and the original equation was derived by Rogers et al. (1984):

$$m_h = \left(\frac{\rho \pi d^2}{4} \right) \frac{(D_e/d)^2 + 1}{(D_e/d)^2 - 1} \tag{2}$$

where ρ is homogeneous mixture density, and D_e is the equivalent diameter to model the confinement due to surrounding tubes. The definitions of D_e for each tube array can be found in Pettigrew et al.'s work (1989a).

3.5 Fluid-Elastic Instability

The most general method to predict the fluid-elastic instability would be Connors' relation which can be formulated in terms of dimensionless "reduced velocity" and "mass damping parameter" as the following equation:

$$\frac{V_{g,c}}{fD} = K \left(\frac{2\pi\zeta m}{\rho D^2} \right)^n \tag{3}$$

where $V_{g,c}$ is the critical gap velocity, f is the tube natural frequency in fluid, ρ is the homogeneous mixture density, m is the mass per unit length (tube mass plus hydrodynamic mass), ζ is the total damping ratio, n is an exponent, and K is the instability constant. The instability constant (K) and the exponent of mass damping parameter (n) should be obtained from the dimensionless "reduced velocity" and "mass damping parameter".

The critical gap velocity could be obtained from the RMS tube displacement curves (Figs.3~5). Damping ratio and hydrodynamic mass values correspond to those measured in the rigid tube bundle at about half the critical gap velocity (Figs. 10 and 11).

As were the results of Pettigrew et al. (1989b), the present results obtained in RT array (p/d = 1.47) showed two regions of instability (Fig. 12). The first region corresponded to lower void fraction region, and n and K had the value of about 0.5 and 3.0 as could be expected from Connors' relation for single phase flow. In the other region at higher void fraction, n had much lower value of around 0.1. For this region, the critical flow velocities were much lower than predicted by the Connors' relation of the former region. The transition between two fluid-elastic instability regions occurred at the void fraction of approximately 80%, which corresponded to the flow regime transition from continuous bubbly flow to intermittent flow.

In the case of NS array (p/d = 1.633), K and n had the value of 6.0 and 0.5, respectively. Pettigrew et al. (1989b) reported that the instability constant was 4.3 for NS array with p/d of 1.47, and they expected that K would be 5.5 for NS array with p/d of 1.633. In addition, the effect of flow regime transition on the fluid-elastic instability behavior was not significant for the NS tube array with p/d of 1.633.

In the case of RS array (p/d = 1.633), K and n had the value of 9.0 and 0.5 for void fraction of 60~70 %. The higher value of K was probably due to the weak tube-to-tube hydrodynamic coupling in two-phase flow condition in the present RS array.

4. CONCLUSIONS

Fluid-elastic instability characteristics in air-water two-phase cross-flow have been experimentally investigated using three different arrays of straight tube bundles. Rotated triangular array tube bundle with p/d of 1.47 is for the counterpart test of Pettigrew et al. (1989a, 1989b). Rotated square and normal square array tube bundles with p/d of 1.633 are for the investigation of fluid-elastic instability features in KSNP steam generator.

Tube vibration response in NS and RT arrays showed strong tube-to-tube hydrodynamic coupling as the gap velocity reached the critical gap velocity. On the other hand, the hydrodynamic coupling between neighboring tubes was very weak in RS array.

The total damping ratios in three tube bundles were very dependent on the void fraction, and had the maximum at void fraction of 60~70%. The hydrodynamic mass ratios in RS array were much lower than those in NS and RT arrays, which might be related with the weak hydrodynamic coupling in RS array.

Fluid-elastic instability in RT array showed two-regions of instability as was in the work of Pettigrew et al. (1989b). In addition, the transition between two fluid-elastic instability regions was closely related with flow regime transition.

The effect of flow regime transition on the fluid-elastic instability behavior was not significant for the NS tube array with p/d of 1.633. K and n had the value of 6.0 and 0.5, respectively.

In the case of RS array, K had the value of 9.0 for void fraction of 60~70 %. The higher value of K was probably due to the weak hydrodynamic coupling in two-phase flow condition.

ACKNOWLEDGEMENTS

The present work has been financially supported by the Ministry of Science and Technology (MOST) of Korean government under the national nuclear mid- & long-term R&D program.

REFERENCES

Carlucci, L. N. and Brown, J. D., (1983), Trans. ASME, Jrnl. of Vibration, Stress and Reliability in Design, Vol. 105, pp. 83~89.

Pettigrew, M. J., Taylor, C. E., and Kim, B. S., (1989a), Trans. ASME, Jrnl. of Pressure Vessel Technology, Vol. 111, pp. 466~477.

Pettigrew, M. J., Tromp, J. H., Taylor, C. E., and Kim, B. S., (1989b), Trans. ASME, Jrnl. of Pressure Vessel Technology, Vol. 111, pp. 478~487.

Pettigrew, M. J., Taylor, C. E., Jong, J. H., and Currie, I. G., (1995), Trans. ASME, Jrnl. of Pressure Vessel Technology, Vol. 117, pp. 321~329.

Pettigrew, M. J., Taylor, C. E., and Kim, B. S., (2001), Trans. ASME, Jrnl. of Pressure Vessel Technology, Vol. 123, pp. 414~420 (2001).

Rogers, R. G., Taylor, C. E., and Pettigrew, M. J., (1984), ASME PVP Conference, San Antonio, Texas, June.

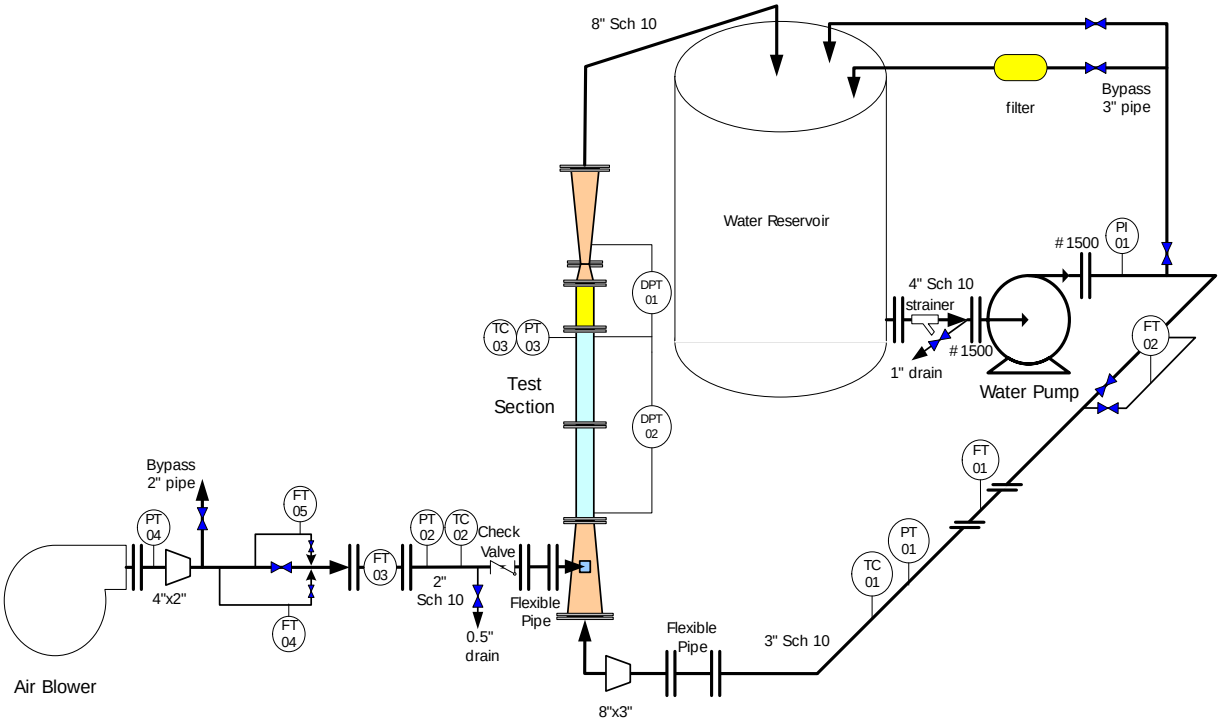

Fig. 1 Schematic of Test Facility

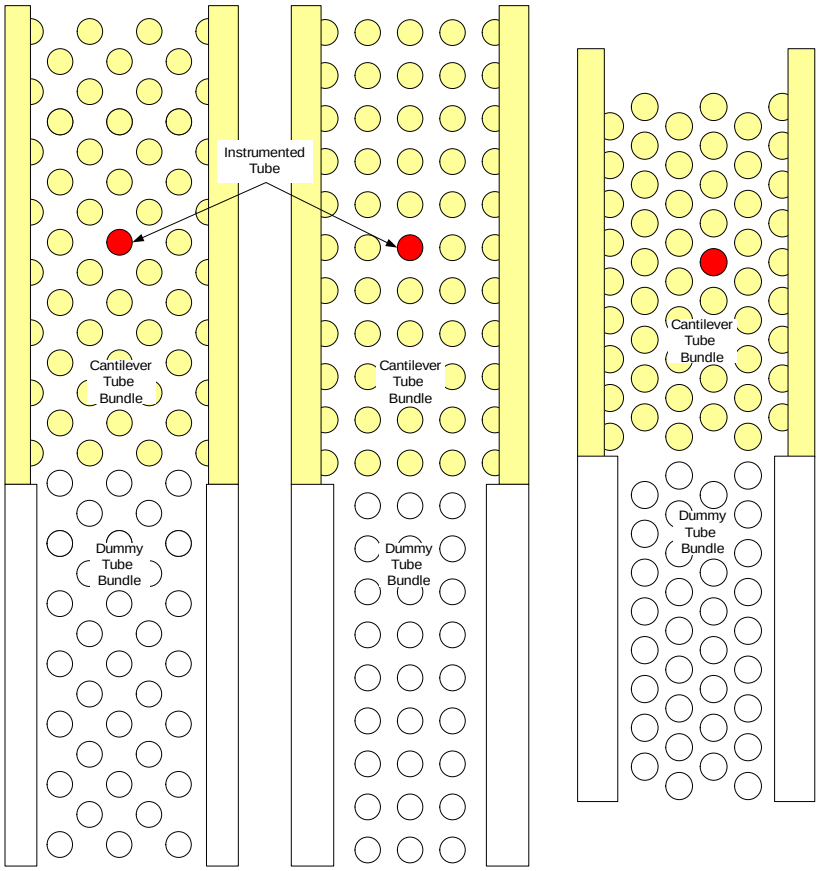

Fig. 2 Tube bundle configurations ; RS (left), NS (center), RT (right) arrays

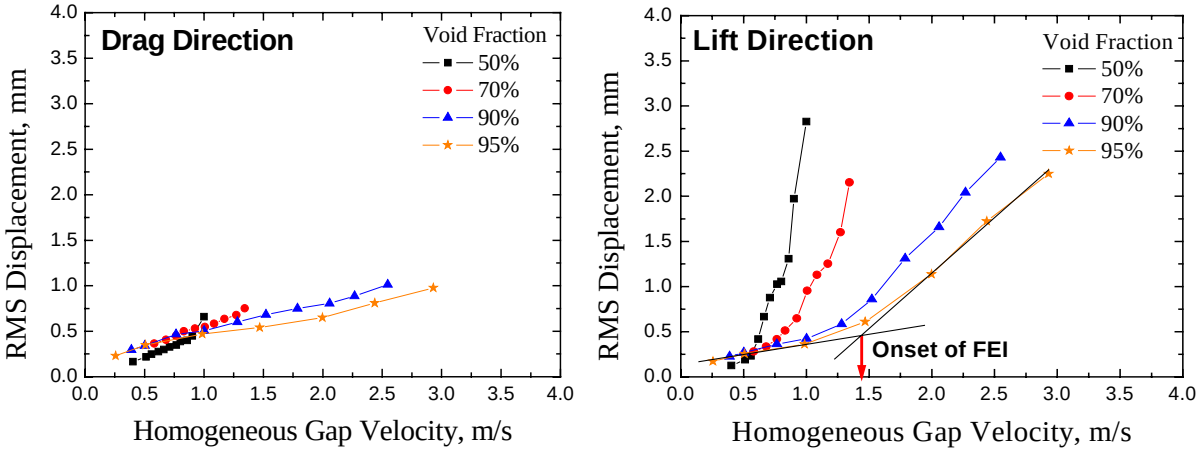

Fig. 3 RMS tube displacement in RT array with P/D of 1.47

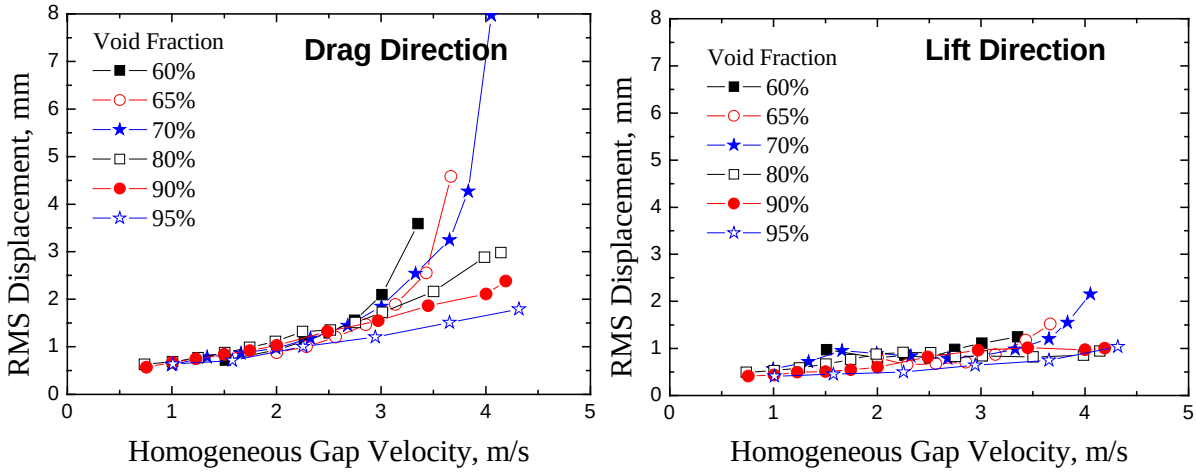

Fig. 4 RMS tube displacement in RS array with P/D of 1.633

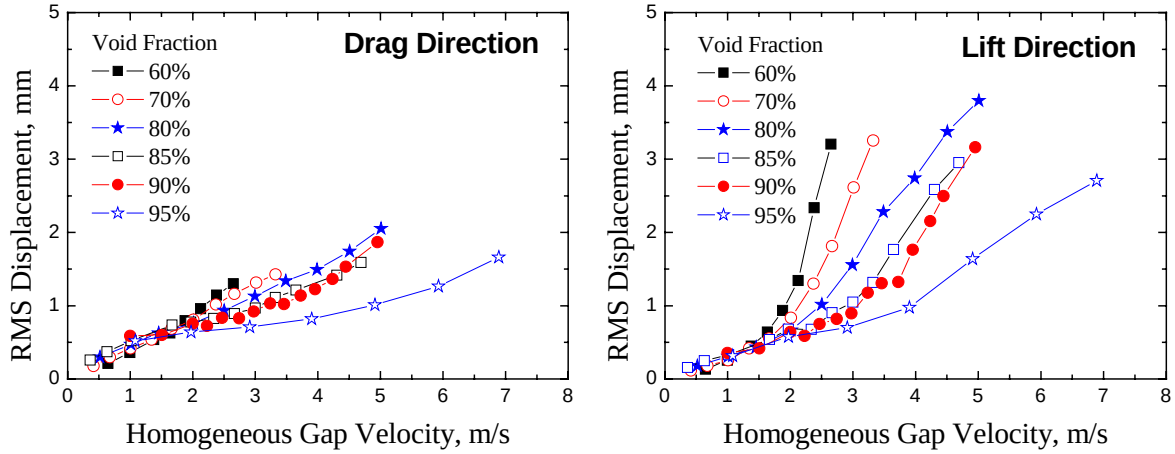

Fig. 5 RMS tube displacement in NS array with P/D of 1.633

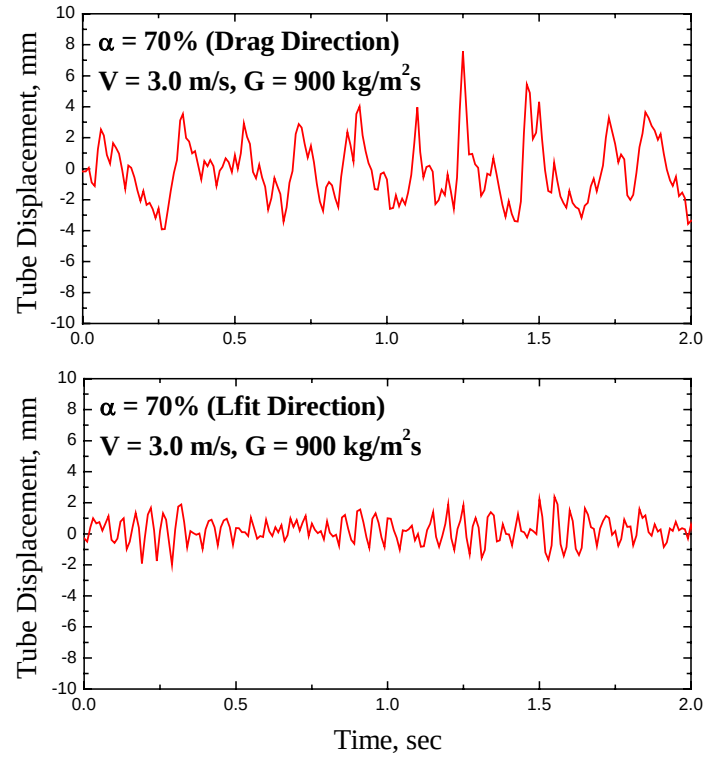

Fig. 6 Tube vibration waveforms in RS array

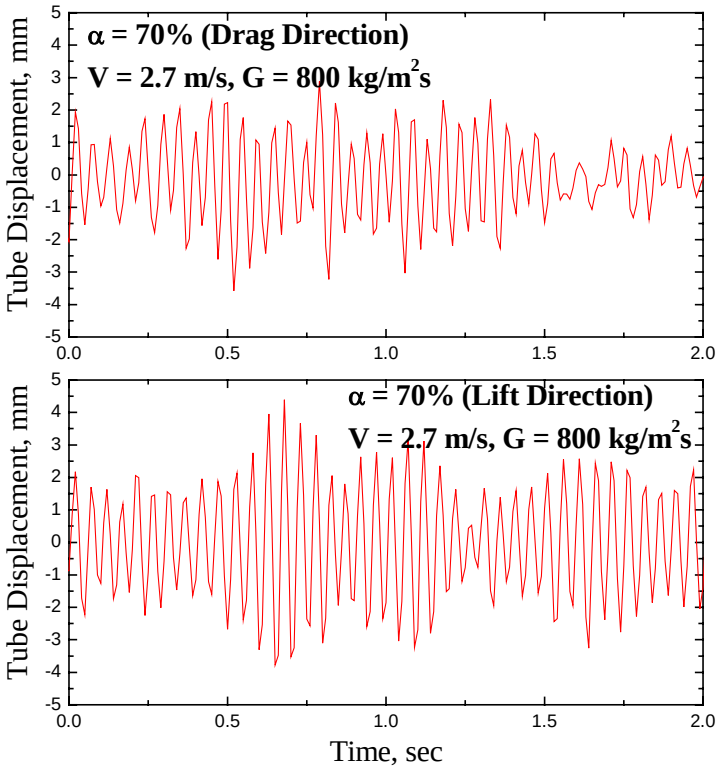

Fig. 7 Tube vibration waveforms in NS array

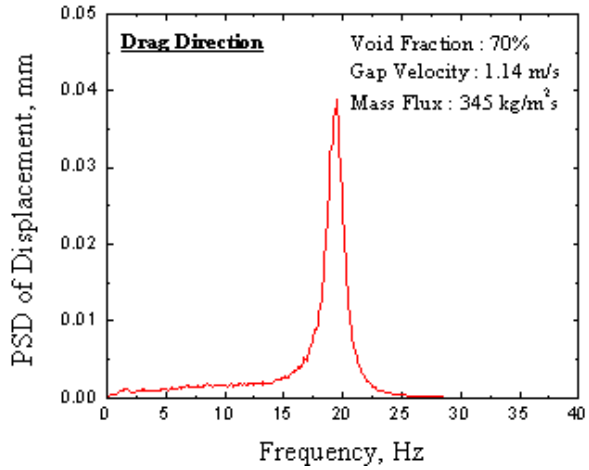

Fig. 8 Typical PSD for tube vibration in NS array

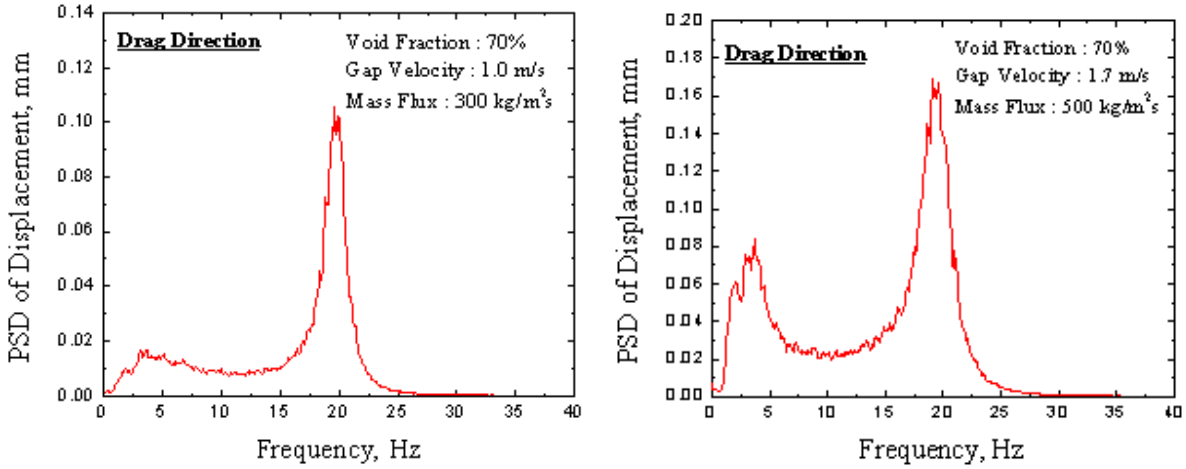

Fig. 9 Typical PSD for tube vibration in RS array

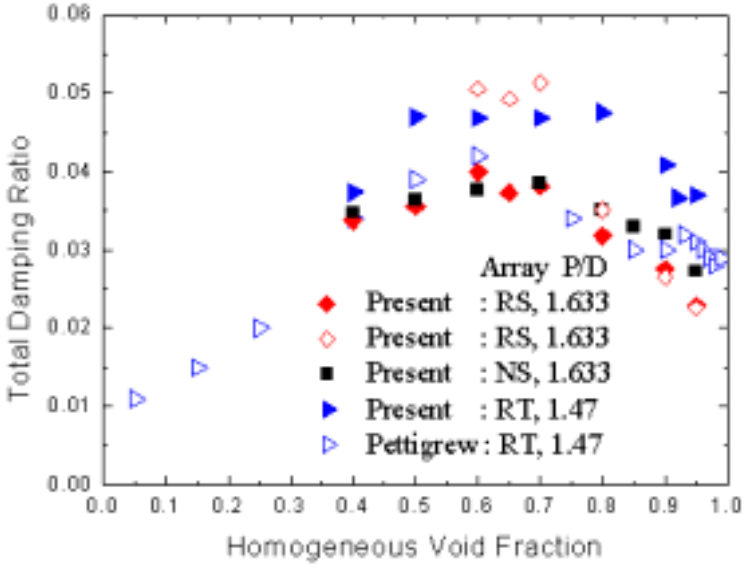

Fig. 10 Total damping ratio (for RS array, ◆: 1/2 of critical gap velocity, ◇: 1/4 of critical gap velocity)

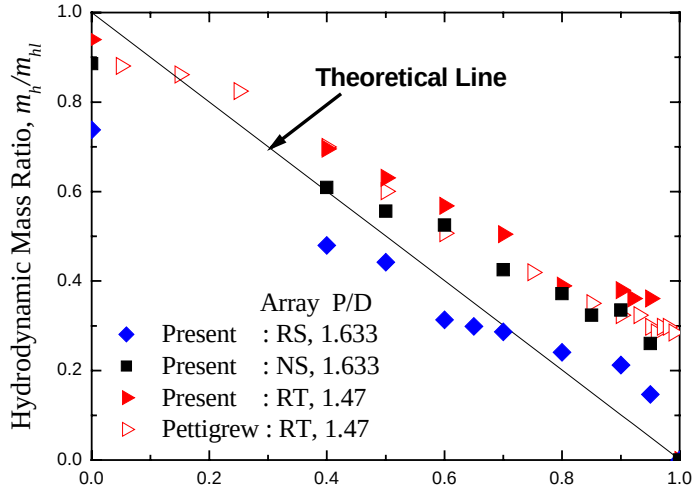

Fig. 11 Hydrodynamic mass ratio

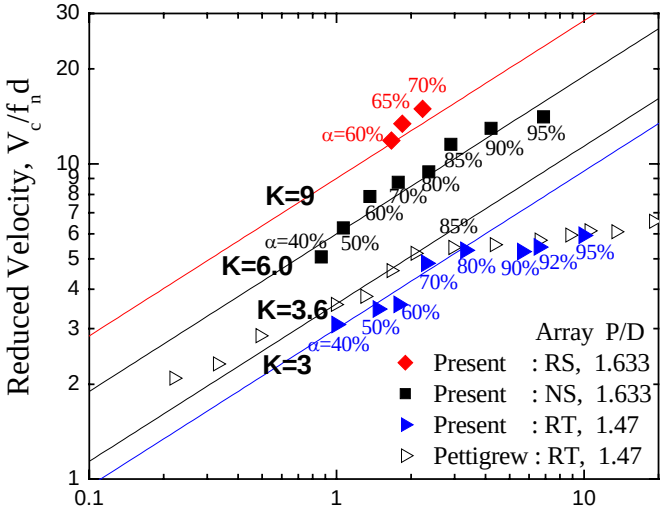

Fig. 12 Fluid-elastic instability results